Implementation of redox gradients in hydrogen bonded complexes containing N,N-dimethylaniline, flavin and fullerene derivatives

ARTICLE *in* JOURNAL OF MATERIALS CHEMISTRY · FEBRUARY 2010

Impact Factor: 7.44 · DOI: 10.1039/b918462g

8 AUTHORS, INCLUDING:

Kei Ohkubo
Osaka University
395 PUBLICATIONS **9,558** CITATIONS
SEE PROFILE

Vito Sgobba
Bayerisches Zentrum für angewandte Ener…
40 PUBLICATIONS **1,777** CITATIONS
SEE PROFILE

Implementation of redox gradients in hydrogen bonded complexes containing *N*,*N*-dimethylaniline, flavin and fullerene derivatives†

Motonobu Murakami,[a] Kei Ohkubo,[a] Taku Hasobe,[b] Vito Sgobba,[c] Dirk M. Guldi,*[c] Florian Wessendorf,[d] Andreas Hirsch*[d] and Shunichi Fukuzumi*[ae]

Received 7th September 2009, Accepted 16th November 2009
First published as an Advance Article on the web 23rd December 2009
DOI: 10.1039/b918462g

A variety of supramolecular complexes were formed by associating an electron donor-substituted flavin dyad (10-[4′-(*N*,*N*-dimethylamino)phenyl]isoalloxazine: **DMA–Fl**) and a family of fullerene derivatives that contain single and double hydrogen bond receptors (**SRC$_{60}$** and **DRC$_{60}$**). The stoichiometry of the corresponding complexes, that is, **DMA–Fl** and **SRC$_{60}$** or **DRC$_{60}$**, were examined by Job's plot analysis of the absorption changes linked to **DMA–Fl** at 470 nm. To this end, 1 : 1 and 1 : 2 complex stoichiometries were determined for **DMA–Fl-SRC$_{60}$** and **(DMA–Fl)$_2$-DRC$_{60}$**, respectively. Molecular aggregates in the form of remarkably stable clusters were formed by the fast injection method. Insights into these clusters came from transmission electron microscopy (TEM) measurements, which revealed network configurations for **(DMA–Fl-SRC$_{60}$)$_n$** with diameters in the range between 200 and 500 nm, while uniform nanoparticles of about 40 nm diameter were discernible for **[(DMA–Fl)$_2$-DRC$_{60}$]$_n$**. The highly colored composite clusters were assembled onto an optically transparent electrode covered with nanostructured SnO_2 films by the electrophoretic deposition technique. Important are the photocurrent action spectra providing maximum IPCE values that are twice as high for **[(DMA–Fl)$_2$-DRC$_{60}$]$_n$** than for **(DMA–Fl-SRC$_{60}$)$_n$**. To complement these studies the dynamics of electron transfer were investigated by femtosecond laser flash photolysis in the supramolecular clusters (*i.e.*, **(DMA–Fl-SRC$_{60}$)$_n$** and **[(DMA–Fl)$_2$-DRC$_{60}$]$_n$**). As a matter of fact, for the first time we were able to demonstrate the unidirectional electron transfer from the terminal electron donor (*N*,*N*-dimethylaniline) moiety to the terminal electron acceptor (fullerene) moiety.

Introduction

Nature has long used several interactions to create formidable arrays of structures, where a great level of control over the organization and an increased flexibility in replacing individual building blocks have been realized.[1] The structure of the bacterial photosynthetic reaction centers provided important insights into the arrangement of electron donors and acceptors, namely the non-covalent incorporation into a well-defined protein matrix.[2] To this end, sunlight is harvested by antenna chlorophyll molecules and is unidirectionally funneled to the special "bacteriochlorophyll dimer" pair. Here, an excited state electron transfer takes place with the consequence that an oxidized special "bacteriochlorophyll dimer" pair is formed, while the electron is inserted into a redox chain. In the latter, unidirectional electron transfer (ET) cascade reactions, which consists of ET without hole transfer, through the well-organized gradients of photosynthetic pigments leads to long-lived charge-separated (CS) states.[2–4] Inspired by the sophistication of the natural photosynthetic systems, multi-step photoinduced intramolecular electron transfer reactions have been a subject of extensive studies.[2–13] In this context, porphyrins with their rich redox properties – in the ground and excited states – have been at the forefront of investigations. In particular, porphyrins emerged as integrative components for the construction of photosynthetic reaction center models, where they act as excited state electron donors. Leading examples comprise several porphyrin–fullerene conjugates starting from a zinc porphyrin–C_{60} dyad (**ZnP–C$_{60}$**),[8] a ferrocene–zinc porphyrin–C_{60} triad (**Fc–ZnP–C$_{60}$**),[9] a zinc porphyrin–free base porphyrin–C_{60} triad, up to a tetrad (**Fc–ZnP–H$_2$P–C$_{60}$**).[10] In all of such multicomponent systems, photoexcitation of the porphyrins is the inception to reduce the terminal electron acceptor and to generate a hole at the porphyrin, followed by hole transfer from the primary donor to the secondary donors *etc*. – leading to the final charge-separated state.[8–13] In contrast, there have been very few examples of multicomponent systems composed of electron donors and

[a]*Department of Material and Life Science, Division of Advanced Science and Biotechnology, Graduate School of Engineering, Osaka University, SORST, Japan Science and Technology Agency (JST), Suita, Osaka, 565-0871, Japan. E-mail: fukuzumi@chem.eng.osaka-u.ac.jp; Fax: +81 6 6879 7370; Tel: +81 6 6879 7368*
[b]*School of Materials Science, Japan Advanced Institute of Science and Technology (JAIST) and PRESTO, JST, Nomi, Ishikawa, 923-1292, Japan*
[c]*Physical Chemistry and Interdisciplinary Center for Molecular Materials (ICMM), FAU Erlangen-Nürnberg, Erlangen, D-91058, Germany. E-mail: guldi@chemie.uni-erlangen.de*
[d]*Organic Chemistry and Interdisciplinary Center for Molecular Materials (ICMM), FAU Erlangen-Nürnberg, Erlangen, D-91054, Germany*
[e]*Department of Bioinspired Science, Ewha Womans University, Seoul, 120-750, Korea*

† Electronic supplementary information (ESI) available: Synthetic protocols and Fig. S1–11. See DOI: 10.1039/b918462g

acceptors, in which a unidirectional flow of electron evolves between the terminal electron donor and the terminal electron acceptor through electron mediators.[14]

Besides porphyrins, flavins – a tricyclic heteronuclear organic ring based on pteridine – are also known to play important roles as electron mediators.[15,16] Importantly, their redox reactivities are finely controlled by hydrogen bonding in, for example, the biological redox systems.[17,18] Flavins, like porphyrins, posses strong absorption bands in the visible region which let them act as photoreceptors.[19] Within the context of photocatalysts for photobiological redox process, photoinduced electron transfer reactions involving flavin turned into a topic of wide interest.[20] Supramolecular electron donor–acceptor complexes linked by hydrogen bonding have merited current interest as functional ensembles to build molecular machines and optoelectronic devices.[21–25] Nevertheless, up to this point there has been no reports on the formation of hydrogen bonded complexes of flavins with electron donors or/and acceptors.

We report herein hydrogen bonded supramolecular assemblies composed of *N*,*N*-dimethylaniline-substituted flavin (10-[4′-(*N*,*N*-dimethylamino)phenyl]isoalloxazine: **DMA–Fl**)[26] and C_{60} derivatives. The latter contain single and double hydrogen bond receptors (**SRC$_{60}$** and **DRC$_{60}$**) as shown in Scheme 1. It is interesting to note that electron transfer reactions with fullerenes are highly efficient owing to the minimal changes that are associated with the structure and solvation in the reduced and/or oxidized state.[27] Importantly, for the first time we provide unambiguous evidence in the new supramolecular system for a multistep electron transfer as oppose to a multistep hole transfer along a fine-tuned and fine-balanced redox gradient. Such a redox gradient implies the systematic and sequential alteration of the redox potential – as inspected by photophysical and electrochemical means – to allow the mediation of charges. The detailed photodynamics were examined by laser flash photolysis measurements. Finally, the **DMA–Fl-SRC$_{60}$** and **(DMA–Fl)$_2$-DRC$_{60}$** complexes were assembled as clusters onto an optically transparent electrode (OTE) covered with nanostructured SnO_2 films (OTE/SnO_2). The photoelectrochemical features of the nanostructured SnO_2 films of **DMA–Fl-SRC$_{60}$** and **(DMA–Fl)$_2$-DRC$_{60}$** clusters are reported in comparison with those of reference systems without flavin.

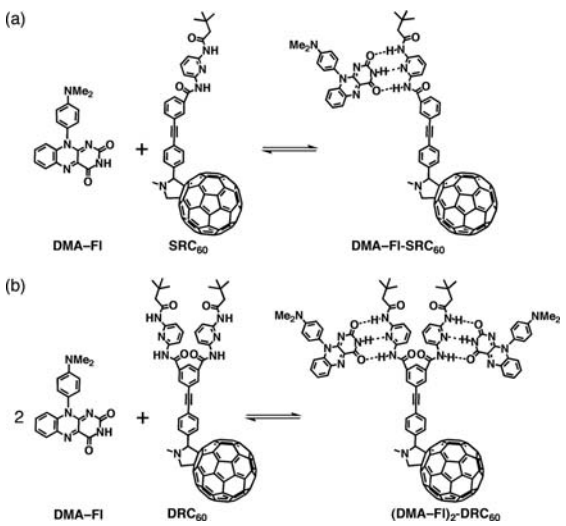

Scheme 1 Formation of supramolecular complex between (a) **DMA–Fl** and **SRC$_{60}$** and (b) **DMA–Fl** and **DRC$_{60}$**.

Experimental

Materials

All chemicals were purchased by chemical suppliers and used without further purification. All analytical reagent-grade solvents were purified by distillation. Dry solvents were prepared using customary literature procedures.[28] Thin layer chromatography (TLC): Riedel–de Haën silicagel F254 and Merck silica gel 60 F254. Detection: UV lamp and iodine chamber. Flash chromatography (FC): Merck silica gel 60 (230–400 mesh, 0.04–0.063 nm). UV-visible spectroscopy: Shimadzu UV-3100 PC UV-visible-NIR scanning spectrophotometer; absorption maxima λ_{max} are given in nm. Mass spectrometry: Micromass Zabspec, FAB (LSIMS) mode, matrix 3-nitrobenzylalcohol. NMR spectroscopy: JEOL JNM EX 400 and JEOL JNM GX 400 and Bruker Avance 300. The chemical shifts are given in ppm relative to TMS. The resonance multiplicities are indicated as s (singlet), d (doublet), t (triplet), q (quartet), quin (quintet) and m (multiplet), non-resolved and broad resonances as br. Elemental analysis (C, H, N): succeeded by combustion and gas chromatographic analysis with an EA 1110 CHNS analyser (CE Instruments). $LiClO_4$ was purchased from Nacalai Tesque, Inc. Tris(2,2′-bipyridine)ruthenium(III) hexafluorophosphate $[Ru(bpy)_3(PF_6)_3]$ was prepared by oxidizing $Ru(bpy)_3^{2+}$ with lead dioxide in aqueous H_2SO_4 followed by the addition of KPF_6.[29] The synthesis of 1-benzyl-1,4-dihydronicotinamide dimer $[(BNA)_2]$ was reported previously.[30] **DMA–Fl** and 10-decylisoalloxazine (reference of **DMA–Fl**) were synthesized according to the literature.[26] Details on the synthetic procedure of DRC_{60} and SRC_{60} are described in the electronic supplementary information (ESI) S1.†

Electrochemical measurements

Measurements of cyclic voltammetry (CV) and differential pulse voltammetry were performed at 298 K using a BAS 630B electrochemical analyzer in a deaerated solvent containing $LiClO_4$ (0.5 mol dm^{-3}) as a supporting electrolyte at 298 K. A conventional three-electrode cell was used with a platinum working electrode and a platinum wire as a counter electrode. The measured potentials were recorded with respect to the Ag/$AgNO_3$ (1.0×10^{-2} mol dm^{-3}). The E_{ox} and E_{red} values (*vs.* Ag/$AgNO_3$) are converted to those *vs.* SCE by adding 0.29 V.[31] All electrochemical measurements were carried out under an atmospheric pressure of argon.

ESR measurements

ESR spectra were taken on a JEOL X-band spectrometer (JES-RE1XE) at 77 K. ESR spectra of the charge-separated state of supramolecular clusters in frozen mixed solvent (hexane–THF (3 : 1, v/v)) and the reduced clusters of fullerene derivatives in frozen mixed solvent (hexane–THF (3 : 1, v/v)) were measured under photoirradiation with a high-pressure mercury lamp (USH–1005D) through a water filter focusing at the sample cell

in the ESR cavity at 77 K. The g value was calibrated using a Mn^{2+} marker. The one-electron oxidized **DMA–Fl** ($DMA^{\bullet+}$–Fl) was generated by the thermal electron-transfer oxidation of **DMA–Fl** with $[Ru(bpy)_3]^{3+}$ in THF. The resulting solution was transferred to a quartz ESR tube under an atmospheric pressure of Ar.

Laser flash photolysis measurements

Femtosecond transient absorption spectroscopy experiments were conducted using an ultrafast source: Integra-C (Quantronix Corp.), an optical parametric amplifier: TOPAS (Light Conversion Ltd.) and a commercially available optical detection system: Helios provided by Ultrafast Systems LLC. The source for the pump and probe pulses were derived from the fundamental output of Integra-C (780 nm, 2 mJ/pulse and fwhm = 130 fs) at a repetition rate of 1 kHz. 75% of the fundamental output of the laser was introduced into TOPAS which has optical frequency mixers, resulting with tunable range from 285 nm to 1660 nm, while the rest of the output was used for white light generation. Prior to generating the probe continuum, a variable neutral density filter was inserted in the path in order to generate stable continuum, then the laser pulse was fed to a delay line that provides an experimental time window of 3.2 ns with a maximum step resolution of 7 fs. In our experiments, a wavelength at 440 nm of TOPAS output, which is the fourth harmonic of signal or idler pulses, was chosen as the pump beam. As this TOPAS output consists of not only the desirable wavelength but also unnecessary wavelengths, the latter was filtered using a wedge prism with a wedge angle of 18°. The desirable beam was irradiated at the sample cell with a spot size of 1 mm diameter where it was merged with the white probe pulse in a close angle (<10°). The probe beam after passing through the 2 mm sample cell was focused on a fiber optic cable that was connected to a CCD spectrograph for recording the time-resolved spectra (410–1200 nm). Typically, 2500 excitation pulses were averaged for 5 s to obtain the transient spectrum at a set delay time. Kinetic traces at appropriate wavelengths were assembled from the time-resolved spectral data. All measurements were conducted at room temperature, 295 K.

Stopped-flow measurements

Transient absorption spectra of the radical cation of *N*,*N*-dimethylaniline-substituted flavin (**DMA–Fl**) were measured during the thermal electron transfer oxidation of **DMA–Fl** with $[Ru(bpy)_3]^{3+}$ (bpy = 2,2′-bipyridine) using a UNISOKU RSP-601 stopped-flow rapid scan spectrophotometer equipped with a MOS-type high sensitive photodiode array under deaerated conditions. The gate time for measurements was set at 2 ms. Typically, deaerated acetonitrile solutions of $[Ru(bpy)_3]^{3+}$ and **DMA–Fl** were transferred to a spectrophotometric cell by means of a glass syringe that had earlier been purged with a stream of argon.

Theoretical calculations

Theoretical calculations were performed with Gaussian03 (Revision C.02, Gaussian, Inc.)[32] on an 8-process Quantum Cube™ developed by the Parallel Quantum Solutions using PM3 molecular orbital method. Graphical outputs of the computational results were generated with the Gauss View software program (ver. 3.09) developed by Semichem, Inc.[33]

Electrophoretic deposition of (DMA–Fl-SRC_{60})$_n$ and [(DMA–Fl)$_2$-DRC_{60}]$_n$ films

A known amount of fullerene derivatives, **DMA–Fl** or a mixed cluster solution in hexane–THF (3 : 1, v/v, 2 cm^3), were transferred to a 1 cm cuvette in which two electrodes (*viz*., OTE/SnO_2 and OTE) were kept at a distance of 6 mm using a Teflon spacer. A dc electronic field (~100 V cm^{-1}) was applied between these two electrodes using a PowerPac HV (Biorad). The deposition of the film can be visibly seen as the solution becomes colourless with simultaneous brown coloration of the OTE/SnO_2 electrode. The UV-visible spectra were recorded on a Perkin Elmer Ramda 750 spectrophotometer. Transmission electron micrographs (TEM) of composite clusters were recorded by applying a drop of the sample to a carbon-coated copper grid. Images were recorded using a Hitachi H7100 transmission electron microscope.

Photoelectrochemical measurements

Photoelectrochemical measurements were carried out in a standard two-compartment cell consisting of a working electrode, and a Pt wire gauze counter electrode. In measurements of a three-compartment cell using a potentiostat, we additionally employed a saturated calomel reference electrode (SCE).[31] This configuration allowed us to carry out photocurrent measurements under electrochemical bias.[34] The detailed measurement information of two- and three electrode systems have been reported previously.[34] A Keithley SourceMeter 2400 was used for recording I–V characteristics and photocurrent generation density. The electrolyte is 0.5 mol dm^{-3} LiI and 5 mmol dm^{-3} I_2 in acetonitrile. A collimated light beam from a 300 W xenon lamp with a AM 1.5 filter was used for excitation of a fullerene–flavin assembly film deposited on an OTE film. In the case of measurements of IPCE spectra, a monochromator (SM-25, Bunkoh-Keiki Co., Ltd.) was introduced into the path of the excitation beam for the selected wavelength.

Results and discussion

Synthesis of fullerene containing the single and double hydrogen bond receptors (SRC_{60} and DRC_{60})

All the donor–acceptor dyads were synthesized in accordance with recent reports.[35] In particular, starting from the 5-halogenerated 1,3-xylenes (X = Br, I) we obtained the corresponding isophthalic acids **1** for the double armed compounds by oxidation reactions using an excess of $KMnO_4$ (Scheme 2). After conversion to the corresponding dichlorides **2** *via* treatment with thionylchloride, coupling with aminopyridine **3** led to the double arm receptors **4** (**X-DR**) in excellent yield. For the synthesis of the single arm receptor we started from commercially available 3-iodobenzoic acid, which was transformed by DCC (dicyclohexylcarbodiimide)/1-HOBT (1-hydroxybenzotriazol) coupling with aminopyridine **3** to give the iodo single arm component **5** (**I-SR**). The aldehyde functionalized precursors **6** and **7** were obtained by Sonogashira coupling of the iodo receptor **4b/5** and 4-ethynyl benzaldehyde in nearly quantitative yields (Scheme 3).

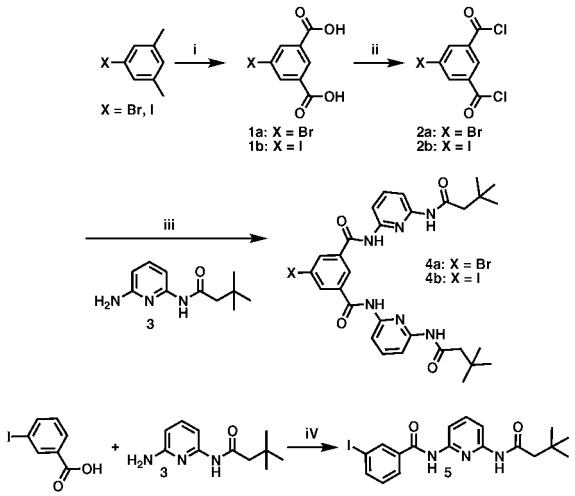

Scheme 2 Syntheses of halogenated Hamilton receptor **4** (**X-DR**) and iodo analogue **5** (**I-SR**): (i) $KMnO_4$, *tert*-butanol/H_2O 1 : 1, 100 °C, 20 h; (ii) $SOCl_2$, DMF, reflux, 6 h; (iii) NEt_3, THF, 0 °C → rt, 12 h; (iv) DCC, DMAP, 1-HOBT, CH_2Cl_2, 0 °C → rt, overnight.

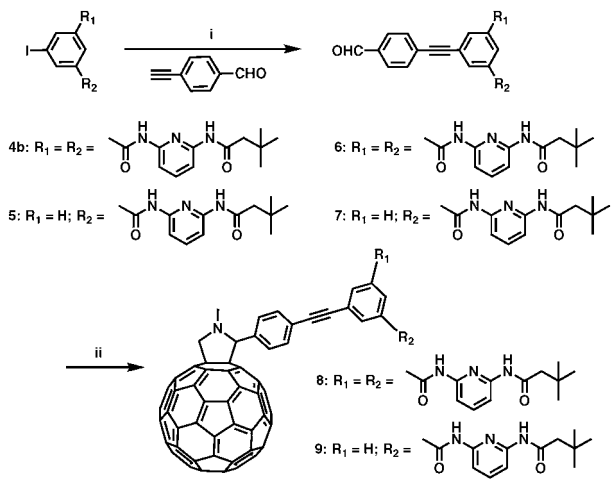

Scheme 3 Syntheses of the Hamilton receptor bearing fullerene monoadducts **8** (**DRC_{60}**) and **9** (**SRC_{60}**): (i) $Pd(PPh_3)_2Cl_2$, CuI, NEt_3, THF, rt, overnight; (ii) C_{60}, sarcosine, THF–toluene, reflux 20 h.

Conversion into the C_{60} monoadducts **8** (**DRC_{60}**) and **9** (**SRC_{60}**) were performed under Prato conditions,[36] that is, excess C_{60}, sarcosine and aldehydes **6** and **7**.

Formation and characterization of supramolecular complex between DMA–Fl and C_{60} derivatives

The single hydrogen bond receptor (**SRC_{60}**) absorbs throughout most of the visible part of the absorption spectrum. Next, a THF solution of the reference compound **5** (**I-SR**) of **SRC_{60}** was titrated to a THF solution of *N*,*N*-dimethylaniline-substituted flavin (**DMA–Fl**) to investigate the formation of the supramolecular complex containing **DMA–Fl** and the hydrogen bond receptor moiety. Importantly, the absorption spectrum changes gradually upon addition of I-SR – see Fig. 1. In fact, a broad

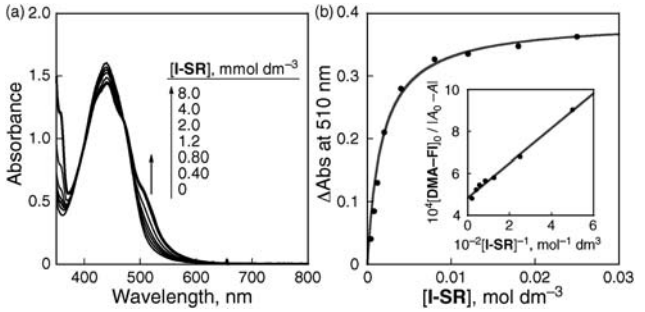

Fig. 1 (a) UV-vis spectral change of **DMA–Fl** (1.9×10^{-4} mol dm^{-3}) in the presence of various concentrations of **I-SR** (0–8 mmol dm^{-3}) in THF. (b) Plots of absorbance change *vs.* [**I-SR**] at 510 nm: plot of $[\mathbf{DMA–Fl}]_0/|A_0 - A|$ *vs.* $[\mathbf{I\text{-}SR}]^{-1}$ at 510 nm for the supramolecular complex formation between **DMA–Fl** and **I-SR**.

absorption band is discernible between 480 and 600 nm. Overall, the absorption changes saturate as the concentration of **I-SR** increases. Implicit is that **I-SR** forms a supramolecular complex with **DMA–Fl**. According to Scheme 4(a), the absorption changes are given by eqn (1),[37]

$$[\mathbf{DMA–Fl}]_0/|A_0 - A| = (\varepsilon_c - \varepsilon_p)^{-1} + (K_1[\mathbf{I\text{-}SR}](\varepsilon_c - \varepsilon_p))^{-1} \quad (1)$$

which assumes a linear correlation between $[\mathbf{DMA–Fl}]_0/|A_0 - A|$ and $[\mathbf{I\text{-}SR}]^{-1}$, where A_0 and A are the absorbance of **DMA–Fl** at 510 nm in the absence and presence of **I-SR**, K_1 is the formation constant of the supramolecular complex between **I-SR** and **DMA–Fl**, and ε_p and ε_c are the molar absorption coefficient of **DMA–Fl** at 510 nm in the absence and presence of **I-SR**, respectively. From the gradient of the linear plot of $[\mathbf{DMA–Fl}]_0/|A_0 - A|$ *vs.* $[\mathbf{I\text{-}SR}]^{-1}$, the formation constant (K_1) was determined as 6.8×10^2 mol^{-1} dm^3 in THF. Similarly, a concentrated THF

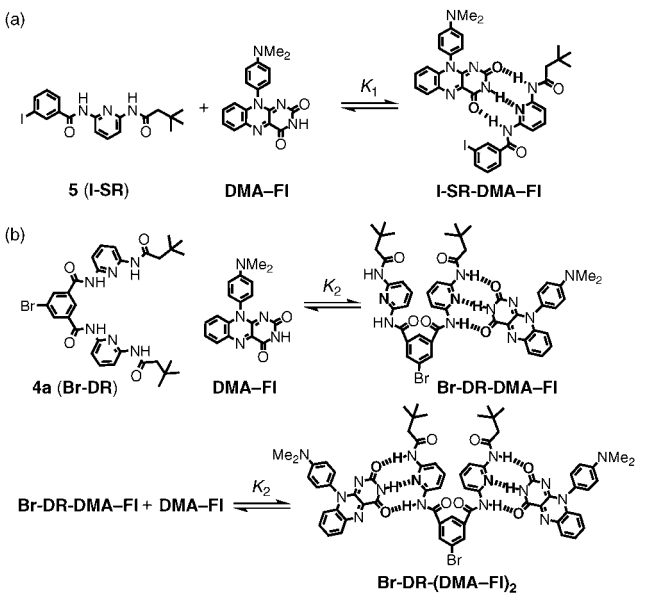

Scheme 4 Formation of the supramolecular complex between (a) **I-SR** and **DMA–Fl** and (b) **Br-DR** and **DMA–Fl**.

solution of the reference compound **4a** (**Br-DR**) of **DRC$_{60}$** was titrated to a THF solution containing **DMA–Fl** to investigate the formation of the supramolecular complex between **DMA–Fl** and **Br-DR** (**Br-DR-(DMA–Fl)$_2$**). Again, the absorption spectrum changes in a single step, that is, revealing a continuous saturation behaviour upon addition of **Br-DR** – see Fig. 2. In the strict sense, the formation of **Br-DR-(DMA–Fl)$_2$** is treated in light of a 1 : 2 complex as is shown in Scheme 4(b).[38] However, the 1 : 2 complex was generated in a single step. This single-step saturation behaviour – Scheme 4(b) – refers to a macroscopic equilibrium eqn (2). From the slope

$$[\mathbf{DMA–Fl}]_0/|A_0 - A| = (\varepsilon_c - \varepsilon_p)^{-1} + (K_2[\mathbf{Br\text{-}DR}](\varepsilon_c - \varepsilon_p))^{-1} \quad (2)$$

of the linear plot of $[\mathbf{DMA–Fl}]_0/|A_0 - A|$ *vs.* $[\mathbf{Br\text{-}DR}]^{-1}$, the formation constant K_2 was determined as 3.9×10^3 mol^{-1} dm^3 in THF.[39] The difference in binding strength between **I-SR-DMA–Fl** and **Br-DR-(DMA–Fl)$_2$** is ascribed to the difference in the number of the involved hydrogen bonds and also to the electronic effect. This led us to optimize the structure of the supramolecular complexes by semiempirical method PM3[32] calculation with Gaussian 03 (see ESI S2†). In fact, **SRC$_{60}$** and **DMA–Fl** seems to interact *via* triple hydrogen bonds, while two contributions, that is, triple hydrogen bonds and π–π interactions, emerge for **DRC$_{60}$** and **DMA–Fl** – see ESI S2.† Interestingly, the strength of both complexes should secure supramolecular complex formation and resembles value found in the literature.[40–42]

The **DMA–Fl-Br-DR** and **DMA–Fl-I-SR** stoichiometries were investigated by the Job's plot analysis using the absorption changes at 470 nm.[43] In this context, the change is given by eqn (3), in which A_T and $(A_T)_R$ are the total absorbance and

$$y = (A_T - (A_T)_R)/((A_T)_{max} - (A_T)_{R,ex}) \quad (3)$$

the reference solution absorbance, $(A_T)_{max} - (A_T)_{R,ex}$ is the maximum absorbance term. The Job's plots showed a maxima at a mole fraction of 0.67 and 0.50 for **DMA–Fl-Br-DR** and **DMA–Fl-I-SR**, respectively, which suggests 2 : 1 and 1 : 1 stoichiometries for the different complexes – see Fig. 3 and ESI S3.†

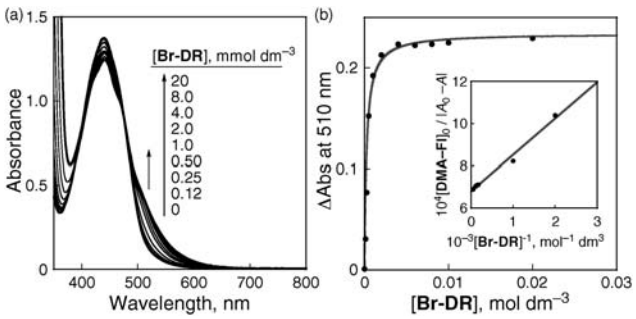

Fig. 2 (a) UV-vis spectral change of **DMA–Fl** (1.6×10^{-4} mol dm^{-3}) in the presence of various concentrations of **Br-DR** (0–20 mmol dm^{-3}) in THF. (b) Plots of absorbance change *vs.* [**Br-DR**] at 510 nm: plot of $[\mathbf{DMA–Fl}]_0/|A_0 - A|$ *vs.* $[\mathbf{Br\text{-}DR}]^{-1}$ at 510 nm for the supramolecular complex formation between **DMA–Fl** and **Br-DR**.

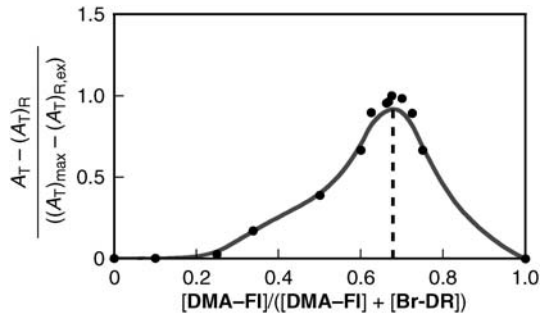

Fig. 3 Job's plot obtained by absorption band at 470 nm for the supramolecular complex formation between **DMA–Fl** and **Br-DR** in THF ($[\mathbf{DMA–Fl}] + [\mathbf{Br\text{-}DR}] = 9.0 \times 10^{-5}$ mol dm^{-3}).

Electrochemical studies and electron-transfer driving force of supramolecular complex between DMA–Fl and DRC$_{60}$

Determination of the redox potentials of the newly formed donor–acceptor hybrids is essential to evaluate, for example, the energetics of electron-transfer reactions and to probe the existence of electron-transfer interactions between the donor and acceptor in the ground state. With this in mind, we have measured the redox potentials of **(DMA–Fl)$_2$-DRC$_{60}$** by means of cyclic voltammetry (CV) and differential pulse voltammetry (DPV) – see experimental section. In deaerated THF containing 0.5 mol dm^{-3} $LiClO_4$, **(DMA–Fl)$_2$-DRC$_{60}$** revealed one-electron

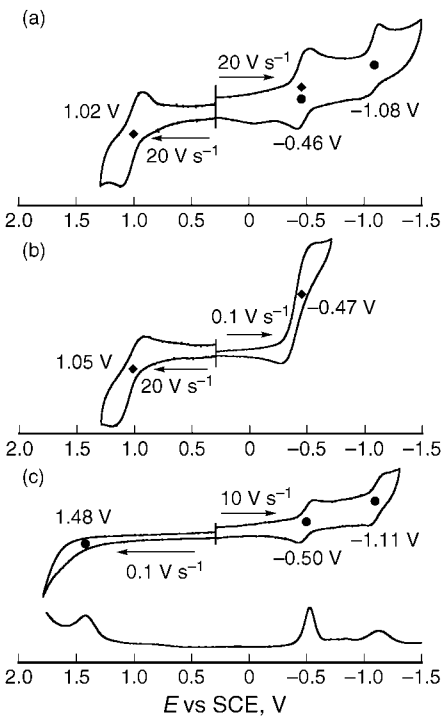

Fig. 4 (a) Cyclic voltammogram (CV) (sweep rate 20 V s^{-1}) with a platinum microelectrode (i.d. 100 μm) of **DMA–Fl** (2.0×10^{-3} mol dm^{-3}) and **DRC$_{60}$** (2.0×10^{-3} mol dm^{-3}), (b) CV (sweep rate 20 and 0.1 V s^{-1}) of **DMA–Fl** (2.0×10^{-3} mol dm^{-3}), and (c) CV (sweep rate 0.1 and 10 V s^{-1}) and differential pulse voltammogram (DPV) (sweep rate 4 mV s^{-1}) of **DRC$_{60}$** (2.0×10^{-3} mol dm^{-3}) in deaerated THF containing $LiClO_4$ (0.5 mol dm^{-3}) at 298 K.

oxidation and one-electron reduction processes at +1.02, −0.46 V *vs*. SCE, respectively (Fig. 4(a)). In accordance with the corresponding references, the one-electron oxidation is likely to involve **DMA–Fl**, while the one-electron reduction occurs at **DRC_{60}** – see Fig. 4(b) and 4(c). Interestingly, in the complex the one-electron oxidation potential is shifted to a lower potential, while that of the one-electron reduction is subject to a shift towards a higher potential. The major conclusion of the electrochemistry is that a photoinduced electron transfer renders easier in the complex than between the individual components. Similarly, the redox potentials of **DMA–Fl-SRC_{60}** and the corresponding constituents – **DMA–Fl**, and **SRC_{60}** – have been measured (see ESI S4†).

Assemblies of supramolecular complexes between DMA–Fl and C_{60} with hydrogen bond receptors as molecular clusters in mixed solvents

DMA–Fl, **SRC_{60}** and **DRC_{60}** are quite soluble in THF and benzonitrile, but sparingly soluble in hexane. When a concentrated THF solution of **DMA–Fl**, **SRC_{60}**, **DRC_{60}**, **DMA–Fl-SRC_{60}** or **(DMA–Fl)$_2$-DRC_{60}** is mixed with hexane by the fast injection method, stable clusters are typically formed.[25b,44] Notable is that the ratio in the mixed solvent is 3 : 1 (v/v) hexane–THF. In particular, we started by mixing solutions of **DMA–Fl** (1 mmol dm^{-3}) and **SRC_{60}** (1 mmol dm^{-3}) or **DMA–Fl** (2 mmol dm^{-3}) and **DRC_{60}** (1 mmol dm^{-3}) in THF (0.5 cm^3). Then, they are injected into a pool of hexane (1.5 cm^3) to form optically transparent composite clusters that are stable at room temperature.

Fig. 5 surveys transmission electron micrograph (TEM) images of the composite clusters: **(DMA–Fl-SRC_{60})**$_n$ and **[(DMA–Fl)$_2$-DRC_{60}]**$_n$. **DMA–Fl-SRC_{60}** seem to self assemble into an interpenetrating network of clusters (*i.e.*, diameter of ~200–500 nm), whereas **(DMA–Fl)$_2$-DRC_{60}** formed uniform nanoparticles (*i.e.*, diameter of ~40 nm). Obviously, the shape and size are largely dependent on the different number of receptors. These trends are further corroborated when inspecting clusters composed of **SRC_{60}** and **DRC_{60}** (see ESI S5†). **(SRC_{60})**$_n$, for example, forms networked clusters (*i.e.*, diameter of ~100–300 nm – see ESI S5(a)†), while uniform nanoparticles are seen for **(DRC_{60})**$_n$ (*i.e.*, diameter of ~30 nm – see ESI, S5(b)†). **(DMA–Fl)**$_n$, on the other hand, forms submicron particles (*i.e.*, diameter of 500 nm −2 μm – see ESI S5(c)†).

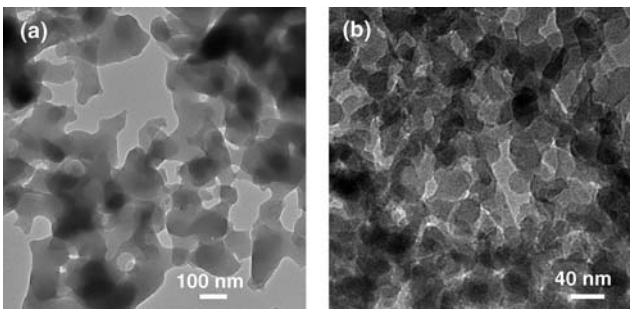

Fig. 5 TEM images of molecular clusters prepared with (a) **[DMA–Fl]** = **[SRC_{60}]** = 0.25 mmol dm^{-3} and (b) **[DMA–Fl]** = 0.50 mmol dm^{-3} and **[DRC_{60}]** = 0.25 mmol dm^{-3} in hexane–THF (3 : 1, v/v).

Electrophoretic deposition

Electrophoretic deposition was applied to fabricate films of clusters (**(DMA–Fl-SRC_{60})**$_n$ and **[(DMA–Fl)$_2$-DRC_{60}]**$_n$) onto OTE and nanostructured SnO_2 films cast onto OTE (OTE/SnO_2).[45,46] A suspension of the clusters (~2 cm^3) in THF was transferred to a 1 cm cuvette. Two OTEs cut from conducting glass were inserted. Then, a dc electric field (~100 V cm^{-1}) was applied. The clusters were driven from the suspension to the positive electrode surface, and a robust thin film was deposited within 2 min. The steady-state absorption spectrum of the OTE/SnO_2/**[(DMA–Fl)$_2$-DRC_{60}]**$_n$ electrode is shown in Fig. 6. The OTE/SnO_2/**[(DMA–Fl)$_2$-DRC_{60}]**$_n$ exhibits much broader absorption in the visible and near-IR regions relative to the **(DMA–Fl)**$_n$ or **(DRC_{60})**$_n$ clusters in a THF–hexane (3 : 1, v/v) mixed solution. This demonstrates that OTE/SnO_2/**[(DMA–Fl)$_2$-DRC_{60}]**$_n$ is a superior light absorber relative to the single component clusters of **(DMA–Fl)**$_n$ or **(DRC_{60})**$_n$.

Photoelectrochemical properties of OTE/SnO_2/(DMA–Fl-SRC_{60})$_n$ and OTE/SnO_2/[(DMA–Fl)$_2$-DRC_{60}]$_n$

Photoelectrochemical measurements were performed in acetonitrile containing LiI (0.5 mol dm^{-3}) and I_2 (5 mmol dm^{-3}) as redox electrolytes with OTE/SnO_2/**[(DMA–Fl)$_2$-DRC_{60}]**$_n$ and OTE/SnO_2/**(DMA–Fl-SRC_{60})**$_n$ as working electrodes and Pt wire as a counter electrode. The photoelectrochemical performance of the OTE/SnO_2/**[(DMA–Fl)$_2$-DRC_{60}]**$_n$ electrode was examined by employing a standard two-compartment cell with a Pt wire gauge counter electrode.[34,47] The photocurrent and photovoltage responses upon exciting OTE/SnO_2/**[(DMA–Fl)$_2$-DRC_{60}]**$_n$ in the visible region (AM 1.5 illumination) are shown in Fig. 7 and 8, respectively. The photocurrent response is prompt, steady and reproducible during repeated on/off cycles of the visible light illumination. The short circuit photocurrent (I_{SC}) of the OTE/SnO_2/**[(DMA–Fl)$_2$-DRC_{60}]**$_n$ electrode is 0.28 mA cm^{-2} (Fig. 7(a)) under white light illumination, that is, AM 1.5 condition and input power: 100 mW cm^{-2}.[48] Remarkably, this value is nearly twice the phocurrent value (0.16 mA cm^{-2}) obtained with the OTE/SnO_2/**(DRC_{60})**$_n$ electrode (Fig. 7(b)). The open circuit voltage (V_{OC}) of the OTE/SnO_2/**[(DMA–Fl)$_2$-DRC_{60}]**$_n$ electrode is 220 mV (Fig. 8(a)) – a value that is identical with that noted for

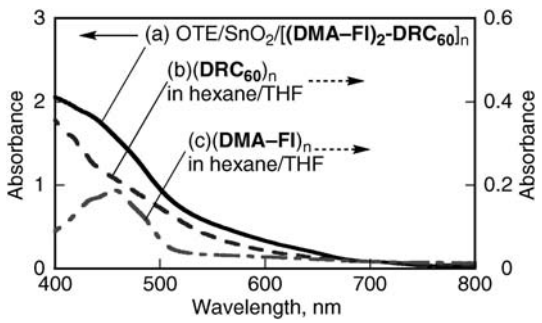

Fig. 6 Absorption spectra of (a) OTE/SnO_2/**[(DMA–Fl)$_2$-DRC_{60}]**$_n$ film prepared from cluster solutions of (**[DMA–Fl]** = 0.50 mmol dm^{-3}, **[DRC_{60}]** = 0.25 mmol dm^{-3}), (b) **(DRC_{60})**$_n$ in hexane–THF (3 : 1, v/v) (**[DRC_{60}]** = 0.25 mmol dm^{-3}) and (c) **(DMA–Fl)**$_n$ in hexane–THF (3 : 1, v/v) (**[DMA–Fl]** = 0.25 mmol dm^{-3}).

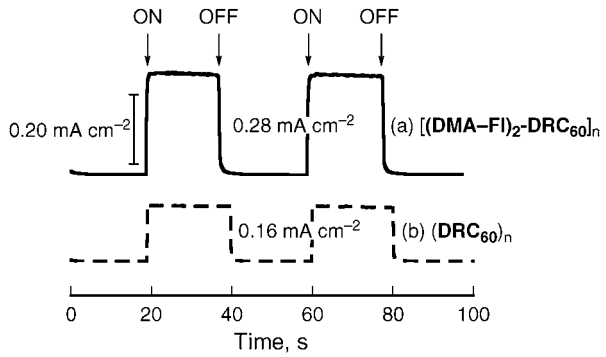

Fig. 7 Photocurrent response of (a) OTE/SnO_2/$[(\mathbf{DMA–Fl})_2\text{-}\mathbf{DRC_{60}}]_n$ and (b) OTE/SnO_2/$(\mathbf{DRC_{60}})_n$ electrode prepared from cluster solution of ($[\mathbf{DMA–Fl}] = 0.50$ mmol dm^{-3}; $[\mathbf{DRC_{60}}] = 0.25$ mmol dm^{-3} to visible light illumination (AM 1.5); electrolyte: LiI (0.5 mol dm^{-3}) and I_2 (5 mmol dm^{-3}) in acetonitrile; input power 100 mW cm^{-2}.

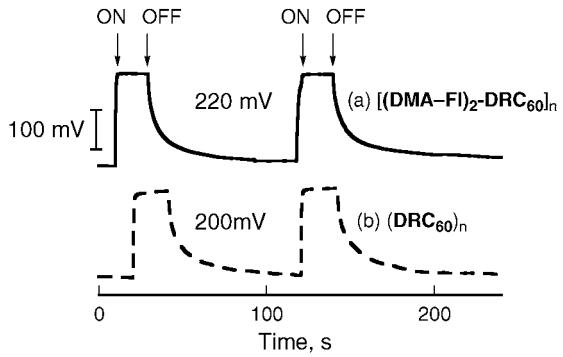

Fig. 8 Photovoltage response of (a) OTE/SnO_2/$[(\mathbf{DMA–Fl})_2\text{-}\mathbf{DRC_{60}}]_n$ and (b) OTE/SnO_2/$(\mathbf{DRC_{60}})_n$ electrode prepared from cluster solution of ($[\mathbf{DMA–Fl}] = 0.50$ mmol dm^{-3}; $[\mathbf{DRC_{60}}] = 0.25$ mmol dm^{-3}) to visible light illumination (AM 1.5); electrolyte: LiI (0.5 mol dm^{-3}) and I_2 (5 mmol dm^{-3}) in acetonitrile; input power 100 mW cm^{-2}.

the OTE/SnO_2/$(\mathbf{DRC_{60}})_n$ electrode (Fig. 8(b)) because the source of the V_{OC} in a photoelectrochemical anodic cell is the difference between the Fermi levels of the redox couple electrolyte and the electron acceptor one. Since they are the same in both systems, the same V_{OC} emerged.

Next, the photocurrent action spectra of the OTE/SnO_2/$[(\mathbf{DMA–Fl})_2\text{-}\mathbf{DRC_{60}}]_n$ and the OTE/SnO_2/$(\mathbf{DMA–Fl\text{-}SRC_{60}})_n$ electrode were evaluated by examining the wavelength dependence of the incident photon to current conversion efficiency (IPCE). The IPCE values are calculated by normalizing the photocurrent densities for the incident light energy, the intensity and the following expression:[34,49]

$$\text{IPCE}(\%) = 100 \times 1240 \times I_{SC}/(W_{in} \times \lambda) \quad (4)$$

where I_{SC} is the photocurrent density (A cm^{-2}), W_{in} is the incident light intensity irradiance (W cm^{-2}), and λ is the excitation wavelength (nm). The photocurrent action spectra of the OTE/SnO_2/$[(\mathbf{DMA–Fl})_2\text{-}\mathbf{DRC_{60}}]_n$ and OTE/SnO_2/$(\mathbf{DMA–Fl\text{-}SRC_{60}})_n$ electrodes are shown in Fig. 9, where they reveal the maximum IPCE values of 5.1% and 3.0% at 440 nm, respectively. The difference in IPCE manifests the importance of uniform

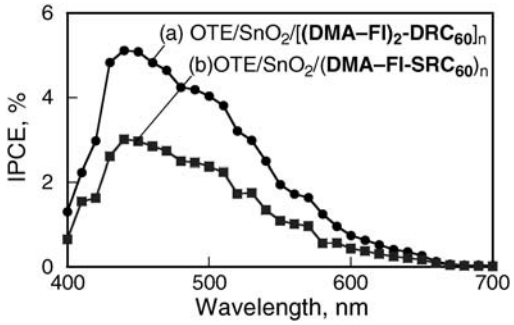

Fig. 9 Photocurrent action spectra (IPCE *vs.* wavelength) of (a) OTE/SnO_2/$[(\mathbf{DMA–Fl})_2\text{-}\mathbf{DRC_{60}}]_n$ electrode prepared from cluster solutions of ($[\mathbf{DMA–Fl}] = 0.50$ mmol dm^{-3}, $[\mathbf{DRC_{60}}] = 0.25$ mmol dm^{-3}) and (b) OTE/SnO_2/$(\mathbf{DMA–Fl\text{-}SRC_{60}})_n$ electrode prepared from cluster solutions of ($[\mathbf{DMA–Fl}] = [\mathbf{SRC_{60}}] = 0.25$ mmol dm^{-3}). Electrolyte LiI (0.5 mol dm^{-3}) and I_2 (5 mmol dm^{-3}) in acetonitrile.

nanoparticle formation and strong hydrogen bonding rather than network structure as means to optimize the cell performance.

The charge separation in the OTE/SnO_2/$[(\mathbf{DMA–Fl})_2\text{-}\mathbf{DRC_{60}}]_n$ electrode is further modulated by applying an electrochemical bias. Here we used a standard three-compartment cell as a working electrode along with Pt wire gauze counter electrode and saturated calomel reference electrode). Fig. 10(a) shows *I–V*

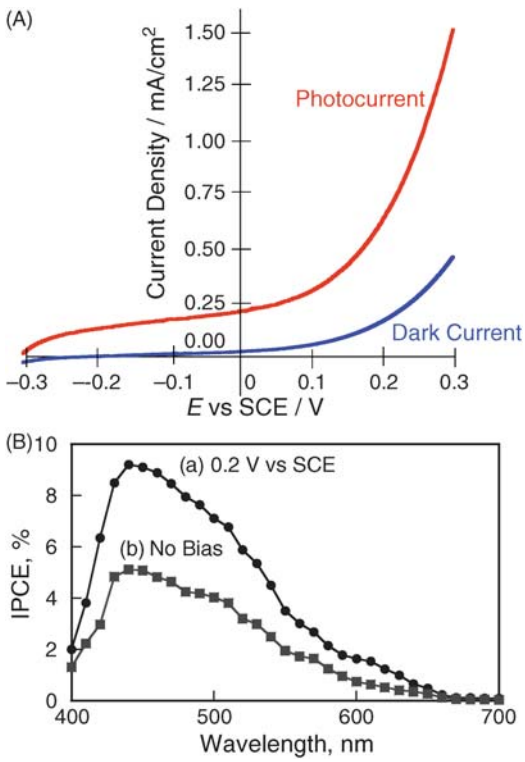

Fig. 10 (a) *I–V* characteristics of the OTE/SnO_2/$[(\mathbf{DMA–Fl})_2\text{-}\mathbf{DRC_{60}}]_n$ electrode under white light illumination (AM 1.5 conditions). Electrolyte: LiI 0.5 mol dm^{-3}, I_2 5 mmol dm^{-3} in acetonitrile; input power = 100 mW cm^{-2}. (b) Photocurrent action spectra (IPCE *vs.* wavelength) of the OTE/SnO_2/$[(\mathbf{DMA–Fl})_2\text{-}\mathbf{DRC_{60}}]_n$ electrode (a) at an applied bias potential of 0.2 V *vs.* SCE and (b) without applied bias potential. Electrolyte: LiI (0.5 mol dm^{-3}), I_2 (5 mmol dm^{-3}) in acetonitrile.

characteristics of the OTE/SnO_2/[**(DMA–Fl)$_2$-DRC$_{60}$**]$_n$ under visible light illumination (AM 1.5). Overall, the photocurrent increases as the applied potential is varied toward more positive potentials. Increased charge separation and facile charge transport under a positive bias potential are responsible for the enhanced photocurrent generation. Notable is that at potentials greater than +0.3 V *vs.* SCE, the direct electrochemical oxidation of iodide interferes with the photocurrent measurement. The net photocurrent generation density of OTE/SnO_2/[**(DMA–Fl)$_2$-DRC$_{60}$**]$_n$ at +0.2 V *vs.* SCE (~0.51 mA cm^{-2}) was much larger than the case at 0 V *vs.* SCE (~0.22 mA cm^{-2}).[46] In summary, controlling the electrochemical bias at OTE/SnO_2 assists in improving the charge separation and in attaining higher IPCE values.[46b]

Finally, the photocurrent action spectra were recorded for OTE/SnO_2/[**(DMA–Fl)$_2$-DRC$_{60}$**]$_n$ under an applied bias of +0.2 V *vs.* SCE. To this end, the maximum IPCE of OTE/SnO_2/[**(DMA–Fl)$_2$-DRC$_{60}$**]$_n$ at +0.2 V *vs.* SCE with 9.2% is nearly twice as large as that measured at 0 V *vs.* SCE (5.1%; spectra in Fig. 10(b)). This trend is in good agreement with the *I–V* characteristics (Fig. 10(a)).

Electron spin resonance (ESR) measurements under photoirradiation

Formation of the one-electron oxidized **DMA–Fl** (**DMA$^{\cdot+}$–Fl**) and the one-electron reduced **DRC$_{60}$** (**DRC$_{60}^{\cdot-}$**) clusters upon photoexcitation of the composite clusters of [**(DMA–Fl)$_2$-DRC$_{60}$**]$_n$ was confirmed by electron spin resonance (ESR) measurements that were performed in frozen hexane–THF at 77 K under photoirradiation. The resulting signal – as shown in Fig. 11(a) – consists of two components: one at a small g value (g = 2.0010) due to **DRC$_{60}^{\cdot-}$** and another one at a higher g value (g = 2.0038) due to **DMA$^{\cdot+}$–Fl**. To confirm these assignments, **DMA$^{\cdot+}$–Fl** and **DRC$_{60}^{\cdot-}$** were produced **Fl** with Ru(bpy)$_3^{3+}$ and by photoinduced electron transfer from dimeric 1-benzyl-1,4-dihydronicotinamide [$(BNA)_2$] to independently by means of the chemical oxidation of **DMA–DRC$_{60}$** clusters,[30] respectively. Their ESR signals are shown in Fig. 11(b) and (c). Overall an excellent agreement is found between the sum of the individually formed radical ion signatures and the photochemically generated radical ion pair. In other words, we accomplished the unambiguous confirmation of **DMA$^{\cdot+}$–Fl** and **DRC$_{60}^{\cdot-}$** in [**(DMA–Fl)$_2$-DRC$_{60}$**]$_n$. Likewise, charge separation was confirmed in (**DMA–Fl-SRC$_{60}$**)$_n$ – see ESI S6.†

Photodynamics of the supramolecular complex clusters between DMA–Fl and C_{60} with hydrogen bond receptors

As a complement to the aforementioned ESR measurements, we employed femtosecond laser flash photolysis performed with the (**DMA–Fl-SRC$_{60}$**)$_n$ and [**(DMA–Fl)$_2$-DRC$_{60}$**]$_n$ clusters as KBr pellets.[50] The incentive of these experiments was – besides an independent spectroscopic characterization of the radical ion pair states – to shed light onto the charge transfer dynamics. In reference experiments with just the bare KBr pellets no detectable changes were noted.

The transient absorption spectra of [**(DMA–Fl)$_2$-DRC$_{60}$**]$_n$ clusters in KBr are shown in Fig. 12(a). Approximately after

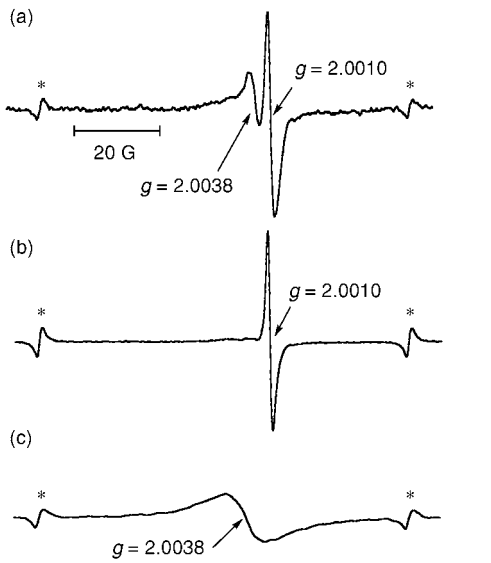

Fig. 11 ESR spectra of (a) photoirradiated [**(DMA–Fl)$_2$-DRC$_{60}$**]$_n$ ([**DMA–Fl**] = 0.50 mmol dm^{-3}; [**DRC$_{60}$**] = 0.25 mmol dm^{-3}) in hexane–THF (3 : 1, v/v) with a high-pressure mercury lamp, (b) the radical anion of **DRC$_{60}$** clusters [(**DRC$_{60}$**)$_n$] (0.50 mmol dm^{-3}) generated in photoinduced electron transfer from dimeric 1-benzyl-1,4-dihydronicotinamide (0.50 mmol dm^{-3}) to **DRC$_{60}$** clusters in hexane–THF (3 : 1, v/v) under photoirradiation of a high-pressure mercury lamp and (c) the radical cation of **DMA–Fl** (0.50 mmol dm^{-3}) produced by the electron transfer oxidation with Ru(bpy)$_3^{3+}$ (0.5 mmol dm^{-3}) in THF, measured at 77 K. Asterisk denotes Mn^{2+} marker.

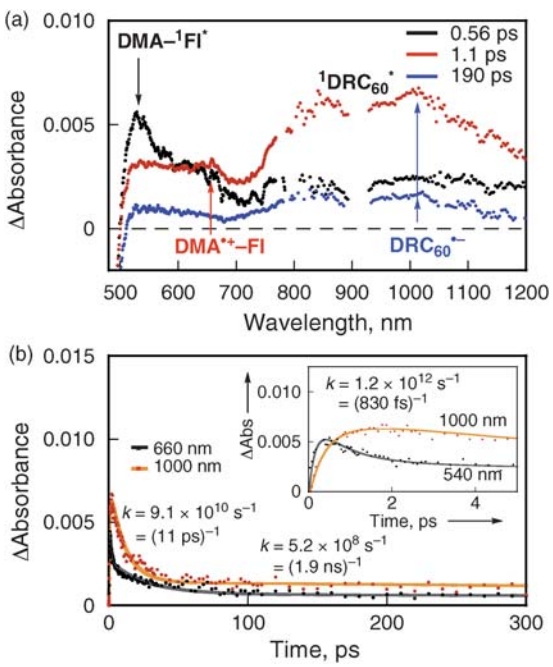

Fig. 12 (a) Transient absorption spectra of [**(DMA–Fl)$_2$-DRC$_{60}$**]$_n$ clusters in KBr pellet taken at 0.56 (black), 1.1 (red) and 190 ps (blue) after femtosecond laser excitation at 440 nm. (b) Time profiles of absorbance at 660 (black) and 1000 nm (red); inset: time profiles at the shorter time range at 540 (black) and 1000 nm (red). The solid curves represent the best fit to the exponential rise or decay.

0.56 ps an absorption maximum develops at 520 nm, which is assigned to the singlet excited state of **DMA–Fl** (**DMA– ^{1}Fl***).[51] The decay of this 520 nm absorption is accompanied by a rise in the absorption at around 1000 nm (inset of Fig. 12(b)). When looking at the transient absorption spectrum at around 1.1 ps the DMA radical cation of **DMA–Fl** (**DMA$^{\cdot+}$–Fl**),[52] radical anion (**DRC$_{60}^{\cdot-}$**)[53] are discernible. The latter radical ion pair is the product of a unidirectional electron transfer (ET) cascade reactions from DMA to C_{60} *via* **DMA–^{1}Fl*** and **^{1}DRC$_{60}^*$**,[54] as summarized in Scheme 5, which determined by photophysical and electrochemical studies. The photoinduced electron transfer (ET) started from the terminal electron-donor (*N*,*N*-dimethylaniline) moiety of **DMA–^{1}Fl*** (2.55 eV) to the terminal electron-acceptor (fullerene) moiety of **(DMA–Fl)$_2$-DRC$_{60}^{\cdot-}$** (1.48 eV) *via* **^{1}DRC$_{60}^*$** (1.75 eV) and **DMA$^{\cdot+}$–Fl$^{\cdot-}$** (1.52 eV). Importantly, the spectroscopic signatures of **DMA$^{\cdot+}$–Fl** and **DRC$_{60}^{\cdot-}$** are still persistent at around 190 ps. The rate constants of photoinduced ET (k_{ET}), charge shift (k_{CS}) and back ET (k_{BET}) were determined as 1.2×10^{12} s^{-1}, 9.1×10^{10} s^{-1} and 5.2×10^{8} s^{-1} by fitting the absorption time profiles at 520 nm (**DMA–^{1}Fl***), 660 nm (**DMA$^{\cdot+}$–Fl**) and 1000 nm (**DRC$_{60}^{\cdot-}$** shown in Fig. 12(b)) with a three-exponential fitting function. Similarly, **(DMA–Fl-SRC$_{60}$)$_n$** was tested by means of time-resolved transient absorption measurements yielding rate constants for photoinduced ET (k_{ET}), charge shift (k_{CS}) and back ET (k_{BET}) of 3.2×10^{12} s^{-1}, 1.4×10^{10} s^{-1} and 8.2×10^{8} s^{-1}, respectively – see ESI S11.†

Conclusions

In summary, a variety of supramolecular complexes were formed by associating an electron donor-substituted flavin dyad (10-[4′-(*N*,*N*-dimethylamino)phenyl]isoalloxazine: **DMA–Fl**) and a family of fullerene derivatives that contain single and double hydrogen bond receptors (**SRC$_{60}$** and **DRC$_{60}$**) with well defined stoichiometries. Importantly, molecular clusters (*i.e.*, **(DMA–Fl-SRC$_{60}$)$_n$** and **[(DMA–Fl)$_2$-DRC$_{60}$]$_n$**) of different size and shape, which were formed by the fast injection method, were assembled onto an optically transparent electrode covered with nanostructured SnO_2 films by electrophoresis. The photoaction spectra providing maximum IPCE values that are twice higher **[(DMA–Fl)$_2$-DRC$_{60}$]$_n$** than for **(DMA–Fl-SRC$_{60}$)$_n$**. As a complement to these studies the dynamics of electron transfer were investigated by femtosecond laser flash photolysis of the supramolecular clusters, which reavealed unidirectional electron transfer (ET) from the terminal electron-donor (*N*,*N*-dimethylaniline) moiety.

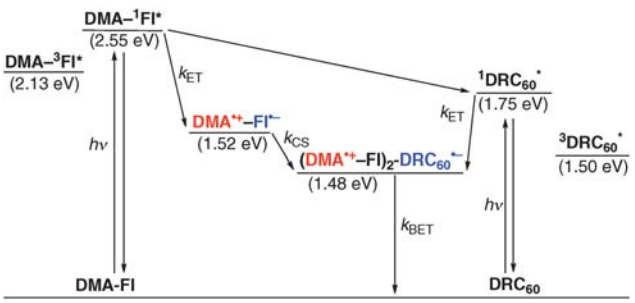

Scheme 5 Energy diagram of **DMA–Fl** and **DRC$_{60}$**.

Acknowledgements

This work was partially supported by KOSEF/MEST through WCU project (R31-2008-000-10010-0), a Grant-in-Aid (Nos. 21750146, 20108010, 19205019 and 19750034) to S.F. and K.O. and a Global COE program, "the Global Education and Research Center for Bio-Environmental Chemistry" to S.F. from the Ministry of Education, Culture, Sports, Science and Technology, Japan. M.M. expresses his special thanks for a Global COE program of Osaka University. Additionally we thank the Deutsche Forschungsgemeinschaft (Exzellenzcluster EAM-Engineering of Advanced Materials) for financial support. T. H. acknowledges Grant-in-Aids for Scientific Research (No. 21710104) and special coordination funds for promoting science and technology from MEXT, Japan.

Notes and references

1 (*a*) G. McDermott, S. M. Priece, A. A. Freer, A. M. Hawthornthwaite-Lawless, M. Z. Papiz, R. J. Cogdell and N. W. Isaaacs, *Nature*, 1995, **374**, 517–521; (*b*) J. Barber, *Nature*, 1988, **333**, 114; (*c*) *Supramolecular Chemistry*, ed. V. Balzani and L. de Cola, NATO ASI Series, Kluwer Academic Publishers, Dordrech, Netherlands, 1992; (*d*) J. W. Steed and J. Atwood, in *Supramol. Chem.* Wiley, Chichester, U.K., 2000; (*e*) V. Balzani, M. Venturini and A. Credi, in *Molecular Devices and Machines*, Wiley-VCH, Weinheim, Germany, 2003; (*f*) G. A. Ozin and A. C. Arsenault, *Nanochemistry*, RSC Publishing: Cambridge, U.K., 2005.

2 C. Kirmaier and D. Holton, in *The Photosynthetic Reaction Center*, ed. J. Deisenhofer and J. R. Norris, Academic Press, San Diego, CA, 1993, vol. II, pp. 49–70.

3 (*a*) A. Remy and K. Gerwert, *Nat. Struct. Biol.*, 2003, **10**, 637–644; (*b*) M. Y. Okumura, M. L. Paddock, M. S. Graige and G. Feher, *Biochim. Biophys. Acta*, 2000, **1458**, 148–163.

4 S. G. Boxer, *Annu. Rev. Biophys. Biophys. Chem.*, 1990, **19**, 267–299.

5 *The Reaction Center of Photosynthetic Bacteria*, ed. M. E. Michel-Beyerle, Springer, Berlin, 1996.

6 (*a*) S. Fukuzumi and H. Imahori, in *Electron Transfer in Chemistry*, ed. V. Balzani, Wiley-VCH, Weinheim, 2001, vol. 2, pp. 927–975; (*b*) S. Fukuzumi and D. M. Guldi, in *Electron Transfer in Chemistry*, ed. V. Balzani, Wiley-VCH, Weinheim, 2001, vol. 2, pp. 270–337; (*c*) S. Fukuzumi, *Org. Biomol. Chem.*, 2003, **1**, 609–620.

7 D. M. Guldi and P. V. Kamat, in *Fullerenes, Chemistry, Physics, and Technology*, ed. K. M. Kadish and R. S. Ruoff, Wiley-Interscience, New York, 2000, pp. 225–281.

8 (*a*) H. Imahori, K. Tamaki, H. Yamada, K. Yamada, Y. Sakata, Y. Nishimura, I. Yamazaki, M. Fujitsuka and O. Ito, *Carbon*, 2000, **38**, 1599–1605; (*b*) S. Fukuzumi, H. Imahori, H. Yamada, M. E. El-Khouly, M. Fujitsuka, O. Ito and D. M. Guldi, *J. Am. Chem. Soc.*, 2001, **123**, 2571–2575.

9 H. Imahori, K. Tamaki, D. M. Guldi, C. Luo, M. Fujitsuka, O. Ito, Y. Sakata and S. Fukuzumi, *J. Am. Chem. Soc.*, 2001, **123**, 2607–2617.

10 H. Imahori, D. M. Guldi, K. Tamaki, Y. Yoshida, C. Luo, Y. Sakata and S. Fukuzumi, *J. Am. Chem. Soc.*, 2001, **123**, 6617–6628.

11 (*a*) H. Imahori, K. Hagiwara, T. Akiyama, M. Aoki, S. Taniguchi, T. Okada, M. Shirakawa and Y. Sakata, *Chem. Phys. Lett.*, 1996, **263**, 545–550; (*b*) N. V. Tkachenko, C. Guenther, H. Imahori, K. Tamaki, Y. Sakata, S. Fukuzumi and H. Lemmetyinen, *Chem. Phys. Lett.*, 2000, **326**, 344–350.

12 V. Vehmanen, N. V. Tkachenko, H. Imahori, S. Fukuzumi and H. Lemmetyinen, *Spectrochim. Acta, Part A*, 2001, **57**, 2229–2244.

13 (*a*) H. Imahori, *Org. Biomol. Chem.*, 2004, **2**, 1425–1433; (*b*) H. Imahori, H. Yamada, D. M. Guldi, Y. Endo, A. Shimomura, S. Kundu, K. Yamada, T. Okada, Y. Sakata and S. Fukuzumi, *Angew. Chem., Int. Ed.*, 2002, **41**, 2344–2347; (*c*) H. Imahori,

K. Tamaki, Y. Araki, Y. Sekiguchi, O. Ito, Y. Sakata and S. Fukuzumi, *J. Am. Chem. Soc.*, 2002, **124**, 5165–5174.
14 M. E. El-Khouly, J. H. Kim, K.-Y. Kay, C. S. Choi, O. Ito and S. Fukuzumi, *Chem.–Eur. J.*, 2009, **15**, 5301–5310.
15 J. Antony, D. M. Medvedev and A. A. Stuchebrukhov, *J. Am. Chem. Soc.*, 2000, **122**, 1057–1065.
16 A. Dirksen, C. J. Kleverlaan, J. N. H. Reek and L. De Cola, *J. Phys. Chem. A*, 2005, **109**, 5248–5256.
17 C. Walsh, *Acc. Chem. Res.*, 1980, **13**, 148–155.
18 V. Massey, *Biochem. Soc. Trans.*, 2000, **28**, 283–296.
19 M. Sun, T. A. Moore and P.-S. Song, *J. Am. Chem. Soc.*, 1972, **94**, 1730–1740.
20 (*a*) S. Fukuzumi and T. Tanaka, in *Photoinduced Electron Transfer*, ed. M. A. Fox and M. Chanon, Elsevier, Amsterdam, 1988, Part C, pp. 636–687; (*b*) S. Fukuzumi, S. Kuroda and T. Tanaka, *J. Am. Chem. Soc.*, 1985, **107**, 3020–3027; (*c*) S. Fukuzumi, K. Yasui, T. Suenobu, K. Ohkubo, M. Fujitsuka and O. Ito, *J. Phys. Chem. A*, 2001, **105**, 10501–10510.
21 A. de la Escosura, M. V. Martínez-Díanz, D. M. Guldi and T. Torres, *J. Am. Chem. Soc.*, 2006, **128**, 4112–4118.
22 (*a*) M. T. Rispens, L. Sánchez, E. H. A. Beckers, P. A. van Hal, A. P. H. J. Schenning, A. El-ghayoury, E. Peeters, E. W. Meijer, R. A. J. Janssen and J. C. Hummelen, *Synth. Met.*, 2004, **135–136**, 801–803; (*b*) E. H. A. Beckers, A. P. H. J. Schenning, P. A. van Hal, A. El-ghayoury, L. Sánchez, J. C. Hummelen, E. W. Meijer and R. A. J. Janssen, *Chem. Commun.*, 2002, 2888–2889; (*c*) L. Sánchez, M. T. Rispens and J. C. Hummelen, *Angew. Chem., Int. Ed.*, 2002, **41**, 838–840.
23 (*a*) F. J. M. Hoeben, P. Johkheijm, E. W. Meijer and A. P. H. J. Schenning, *Chem. Rev.*, 2005, **105**, 1491–1546; (*b*) T. Konishi, A. Ikeda and S. Shinkai, *Tetrahedron*, 2005, **61**, 4881–4899; (*c*) R. Bonnett and G. Martínez, *Tetrahedron*, 2001, **57**, 9513–9547.
24 (*a*) A. Lavie-Cambot, M. Cantuel, Y. Leydet, G. Jonusauskas, D. M. Bassani and N. D. McClenaghan, *Coord. Chem. Rev.*, 2008, **252**, 2572–2584; (*b*) C.-H. Huang, N. D. McClenaghan, A. Kuhn, J. W. Hofstraat and D. M. Bassani, *Org. Lett.*, 2005, **7**, 3409–3412.
25 (*a*) T. Hasobe, K. Saito, P. V. Kamat, V. Troiani, H. Qiu, N. Solladié, K. S. Kim, J. K. Park, D. Kim, F. D'Souza and S. Fukuzumi, *J. Mater. Chem.*, 2007, **17**, 4160–4170; (*b*) T. Hasobe, P. V. Kamat, M. A. Absalom, Y. Kashiwagi, J. Sly, M. J. Crossley, K. Hosomizu, H. Imahori and S. Fukuzumi, *J. Phys. Chem. B*, 2004, **108**, 12865–12872.
26 W. B. Cowden, P. K. Halladay, R. B. Cunningham, N. H. Hunt and I. A. Clark, *J. Med. Chem.*, 1991, **34**, 1818–1822.
27 (*a*) D. M. Guldi and K.-D. Asmus, *J. Am. Chem. Soc.*, 1997, **119**, 5744–5745; (*b*) S. Fukuzumi, K. Ohkubo, H. Imahori and D. M. Guldi, *Chem.–Eur. J.*, 2003, **9**, 1585–1593.
28 W. L. F. Armarego and C. L. L. Chai, in *Purification of Laboratory Chemicals 5th Edition*, Elsevier, London, 2003.
29 R. E. DeSimone and R. S. Drago, *J. Am. Chem. Soc.*, 1970, **92**, 2343–2352.
30 S. Fukuzumi, T. Suenobu, M. Patz, T. Hirasaka, S. Itoh, M. Fujitsuka and O. Ito, *J. Am. Chem. Soc.*, 1998, **120**, 8060–8068.
31 C. K. Mann and K. K. Barnes, in *Electrochemical Reactions in Non-aqueous Systems*, Mercel Dekker, New York, 1970.
32 (*a*) J. J. P. Stewart, *J. Comput. Chem.*, 1989, **10**, 209–220; (*b*) J. J. P. Stewart, *J. Comput. Chem.*, 1989, **10**, 221–264.
33 R. Dennington II, T. Keith, J. Millam, K. Eppinnett, W. L. Hovell and R. Gilliland, Semichem, Inc., Shawnee Mission, KS, 2003.
34 G. Pagona, A. S. D. Sandanayaka, T. Hasobe, G. Charalambidis, A. G. Coutsolelos, M. Yudasaka, S. Iijima and N. Tagmatarchis, *J. Phys. Chem. C*, 2008, **112**, 15735–15741.
35 F. Wessendorf and A. Hirsch, *Tetrahedron*, 2008, **64**, 11480–11489.
36 M. Prato and M. Maggini, *Acc. Chem. Res.*, 1998, **31**, 519–526.
37 S. Fukuzumi, Y. Kondo, S. Mochizuki and T. Tanaka, *J. Chem. Soc., Perkin Trans. 2*, 1989, 1753–1761.
38 (*a*) K. A. Connors, *Chem. Rev.*, 1997, **97**, 1325–1357; (*b*) K. A. Connors, A. Paulson and D. Toledo-Velasquez, *J. Org. Chem.*, 1988, **53**, 2023–2026.
39 The solubilities of C_{60} derivatives and flavin derivatives are not enough to observe the supramolecular formation by ^{1}H NMR, thus we cannot show the ^{1}H NMR data.
40 (*a*) A. Niemz and V. M. Rotello, *Acc. Chem. Res.*, 1999, **32**, 44–52; (*b*) A. K. Boal and V. M. Rotello, *J. Am. Chem. Soc.*, 1999, **121**, 4914–4915; (*c*) E. C. Breinlinger, C. J. Keenan and V. M. Rotello, *J. Am. Chem. Soc.*, 1998, **120**, 8606–8609; (*d*) M. D. Greaves and V. M. Rotello, *J. Am. Chem. Soc.*, 1997, **119**, 10569–10572; (*e*) R. Deans and V. M. Rotello, *J. Org. Chem.*, 1997, **62**, 4528–4529.
41 (*a*) J. Schmidt, R. Schmidt and F. Würthner, *J. Org. Chem.*, 2008, **73**, 6355–6362; (*b*) R. M. Cowie, S. M. Turega and D. Philp, *Org. Lett.*, 2006, **8**, 5179–5182; (*c*) M. H. Al-Sayah and N. R. Branda, *Org. Lett.*, 2002, **4**, 881–884; (*d*) D. M. Guldi, G. M. A. Rahman, M. Prato, N. Jux, S. Qin and W. Ford, *Angew. Chem., Int. Ed.*, 2005, **44**, 2015–2018.
42 (*a*) F. Wessendorf, J.-F. Gnichwitz, G. H. Sarova, K. Hager, U. Hartnagel, D. M. Guldi and A. Hirsch, *J. Am. Chem. Soc.*, 2007, **129**, 16057–16071; (*b*) K. Hager, A. Franz and A. Hirsch, *Chem.–Eur. J.*, 2006, **12**, 2663–2679; (*c*) K. Maurer, K. Hager and A. Hirsch, *Eur. J. Org. Chem.*, 2006, 3338–3347.
43 W. Likussar and D. F. Boltz, *Anal. Chem.*, 1971, **43**, 1265–1272.
44 (*a*) T. Hasobe, H. Imahori, P. V. Kamat, T. K. Ahn, S. K. Kim, D. Kim, A. Fujimoto, T. Hirakawa and S. Fukuzumi, *J. Am. Chem. Soc.*, 2005, **127**, 1216–1228; (*b*) P. V. Kamat, S. Barazzouk, K. G. Thomas and S. Hotchandani, *J. Phys. Chem. B*, 2000, **104**, 4014–4017; (*c*) P. K. Sudeep, B. I. Ipe, K. G. Thomas, M. V. George, S. Barazzouk, S. Hotchandani and P. V. Kamat, *Nano Lett.*, 2002, **2**, 29–35; (*d*) P. V. Kamat, S. Barazzouk, S. Hotchandani and K. G. Thomas, *Chem.–Eur. J.*, 2000, **6**, 3914–3921.
45 S. Barazzouk, S. Hotchandani, K. Vinodgopal and P. V. Kamat, *J. Phys. Chem. B*, 2004, **108**, 17015–17018.
46 T. Hasobe, H. Imahori, S. Fukuzumi and P. V. Kamat, *J. Phys. Chem. B*, 2003, **107**, 12105–12112.
47 H. Imahori, T. Hasobe, H. Yamada, P. V. Kamat, S. Barazzouk, M. Fujitsuka, O. Ito and S. Fukuzumi, *Chem. Lett.*, 2001, 784–785.
48 $(DMA–FI-SRC_{60})_n$ based photoelectrochemical cells showed lower photocurrent conversion when compared with $[(DMA–FI)_2$-$DRC_{60}]_n$ ones as shown in the photocurrent action spectra in Fig. 9.
49 T. Hasobe, Y. Kashiwagi, M. A. Absalom, J. Sly, K. Hosomizu, M. J. Crossley, H. Imahori, P. V. Kamat and S. Fukuzumi, *Adv. Mater.*, 2004, **16**, 975–979.
50 T. Kojima, T. Nakanishi, R. Harada, K. Ohkubo, S. Yamaguchi and S. Fukuzumi, *Chem.–Eur. J.*, 2007, **13**, 8714–8725.
51 The transient absorption band at 520 nm is assigned to the singlet excited state of the Fl moiety by comparison with that of reference compound of DMA–Fl (the singlet excited state of 10-decylisoalloxazine) (see ESI, S7†).
52 The CV of DMA–Fl in deaerated benzonitrile shows an irreversible oxidation wave at a low scan rate (0.1 V s^{-1}), while above 50 V s^{-1}, it exhibits a reversible oxidation-reduction couple. Thus, $DMA^{\bullet+}$–Fl was detected in the thermal electron transfer oxidation of DMA–Fl with $[Ru(bpy)_3]^{3+}$ by using a stopped-flow method (see Experimental Section) in millisecond timescale (see ESI, S8†).
53 The one-electron reduced species of DRC_{60} ($DRC_{60}^{\bullet-}$) is stable in deaerated benzonitrile. $DRC_{60}^{\bullet-}$ was produced by the photochemical reduction of DRC_{60} with $(BNA)_2$ (see ESI, S9†).
54 The broad transientabsorption band at around 900 nm is assigned to the singlet excited state of the C_{60} moiety by comparison with that of $^1DRC_{60}^*$ (see ESI, S10†).

